# Elevated Lipid Infiltration Is Associated With Cerebral Aneurysm Rupture

Chubin Ou[1], Yi Qian[2], Xin Zhang[1], Jiahui Liu[1], Wenchao Liu[1], Hengxian Su[1], Nan Zhang[1], Jianbo Zhang[1], Xuying He[1]* and Chuan-Zhi Duan[1]*

[1] Guangdong Provincial Key Laboratory on Brain Function Repair and Regeneration, Department of Neurosurgery, National Key Clinical Specialty, Engineering Technology Research Center of Education Ministry of China, Neurosurgery Institute, Zhujiang Hospital, Southern Medical University, Guangzhou, China, [2] Department of Biomedical Sciences, Faculty of Medicine and Health Sciences, Macquarie University, Sydney, NSW, Australia

**Background:** Intracranial aneurysm wall degradation can be associated with lipid infiltration. However, the relationship between lipid infiltration and aneurysm rupture has not been explored quantitatively. To investigate the correlation between lipid infiltration and aneurysm rupture, we utilized patient-specific simulation of low-density lipoprotein (LDL) transport to analyze lipid infiltration in the cerebral aneurysm wall.

**Methods:** Sixty-two aneurysms were analyzed. Patient blood pressure, plasma LDL concentration, and three-dimensional angiographic images were obtained to simulate LDL transport in aneurysms. Morphological, hemodynamic, and lipid accumulation parameters were compared between ruptures and unruptured groups. Multivariate logistic regression was also performed to determine parameters that are independently associated with rupture.

**Results:** Size ratio, wall shear stress, low shear area, relative residence time, area-averaged LDL infiltration rate, and maximum LDL infiltration rate were significant parameters in univariate analysis ($P < 0.05$). Multivariate analysis revealed that only average LDL infiltration remained as a significant variable ($P < 0.05$). The prediction model derived showed good performance for rupture prediction (AUC, 0.885; 95% CI, 0.794–0.976).

**Conclusions:** Ruptured aneurysms showed significantly higher LDL infiltration compared to unruptured ones. Our results suggested that lipid infiltration may promote aneurysm rupture. Lipid infiltration characteristics should be considered when assessing aneurysm rupture risk.

Keywords: hemodynamics, intracranial aneurysm, subarachnoid hemorrhage, low-density lipoproteins, computer simulation

## BACKGROUND

Intracranial aneurysms were present in 3–7% of the population (1). Given the high prevalence and catastrophic consequence of rupture, early detection of aneurysms at high risk is vital. Morphological and hemodynamic parameters have been shown to be associated with aneurysm rupture (2–7), yet there is still debate on the role of wall shear stress in aneurysm rupture (8). It has

also been shown that aneurysm wall degradation is associated with lipid accumulation (9–11) and the use of a lipid-lowering agent can reduce the risk of rupture (12). As aneurysm wall degradation is closely related to lipid accumulation, evaluating lipid accumulation in aneurysmal wall might provide extra information for rupture prediction. However, it is relatively difficult to measure lipid accumulation quantitatively in cerebral aneurysm *in vivo*, which limits its use in clinical settings. The simulation of low-density lipoprotein (LDL) transport in diseased arteries has demonstrated its capability in the prediction of lipid infiltration and subsequent plaque progression (13, 14). This has brought us to consider using simulation to evaluate lipid infiltration in the aneurysmal wall and its potential use in rupture prediction.

In this study, we used patient-specific simulation to evaluate the amount of LDL infiltration into the aneurysmal wall and analyzed the difference between ruptured and unruptured aneurysms. Our aim was to investigate the association between LDL infiltration and aneurysm rupture.

## METHODS

### Patient Selection

The data in the current study were obtained from a single center. Approval for this study was obtained from the local institutional review board. The data were anonymous, and the requirement for informed consent was therefore waived. All patients had at least one aneurysm confirmed by three-dimensional digital subtraction angiography (DSA). Patient cases with poor image quality or incomplete record of lipid level were excluded.

### Evaluation of Morphologic Characteristics

Morphological parameters including aneurysm size, aneurysm height, aneurysm width, neck width, vessel angle, aspect ratio (AR), and size ratio (SR) were measured and calculated from three-dimensional reconstructed images according to the definition in previous research (15). Measurements were done by experienced neurosurgeons who were blinded to the status of aneurysms.

### Evaluation of Hemodynamic and LDL Infiltration Characteristics

Each aneurysm model was segmented and reconstructed using MIMICS software (Materialize). The reconstructed three-dimensional models were meshed using ANSYS ICEM CFD software (ANSYS Inc) to create a finite volume mesh composed of tetrahedral elements and prism elements at the wall boundary. Blood was assumed as incompressible Newtonian fluid governed by Navier–Stokes equations. LDL transport in blood was driven by flow convection and diffusion. The modeling of LDL transport was based on previous work, which has been validated

**Abbreviations:** LDL, low-density lipoprotein; WSS, normalized wall shear stress; MWSS, maximum normalized wall shear stress; OSI, oscillatory shear index; LSA, low shear area; RRT, relative residence time; CFD, computational fluid dynamics; AR, aspect ratio; SR, size ratio; LIave, area-averaged normalized lipid infiltration rate; LImax, maximum normalized lipid infiltration rate; ROC, receiver operating characteristic curve; AUC, area under the curve.

(16, 17). LDL transport was governed by the convection–diffusion equation:

$$\frac{\partial C}{\partial t} + U \cdot \nabla C - D\Delta C = 0$$

where U is the blood flow velocity vector, C is the concentration of LDL, and D is the diffusion coefficient. The permeation of LDL across the endothelial membrane was through vesicular pathway and leaky junctions on endothelium. Since the distribution pattern of LDL concentration in the wall is very similar to that of LDL flux across endothelium (16), in this study, we neglected the distribution of LDL inside the wall and focused on its infiltration across the endothelium. The apparent permeability of endothelium was mediated by local wall shear stress and pressure. We used pore theory to estimate the LDL infiltration rate across the endothelium, which was calculated with local LDL concentration in blood flow, local permeability, and transmural pressure difference.

$$J_s = (P_v + P_{app,lj})C$$
$$P_{app,lj} = P_{lj}Z_{lj} + J_{v,lj}(1 - \sigma_f)$$
$$P_{lj} = f(P, WSS, a, D), \quad J_{v,lj} = g(P, WSS)$$

where $P_{app}$ is the apparent permeability of the endothelium composed of $P_v$, the permeability of the vesicular pathway, and $P_{app,lj}$, the permeability of the leaky junction, which is determined by the diffusion effect $P_{lj}$ and convection effect $J_{v,lj}$. The diffusion flux $P_{lj}$ is affected by LDL particle radius a, diffusivity D, and the area density of leaky junctions, which is dependent on local shear stress and local transmural pressure. Similarly, the convection flux $J_{v,lj}$ is determined by the area density of leaky junctions, which is dependent on local shear stress and local transmural pressure. In summary, the LDL infiltration rate was dependent on LDL particle size, diffusivity, local shear stress, local transmural pressure, and local concentration of LDL.

The methodology was presented in detail in previous work (16–18). Physiologic pulsatile flow and patient-specific LDL concentration were prescribed at inlets, and no-slip boundary conditions were applied at vessel walls. Hemodynamic parameters including normalized time-averaged wall shear stress (WSS), normalized maximum wall shear stress (MWSS), low shear area (LSA), oscillatory shear index (OSI), and relative residence time (RRT) were calculated according to the definition presented in the literature (2). The degree of LDL infiltration was evaluated by two parameters, which are area-averaged LDL infiltration rate (LIave) and maximum LDL infiltration rate (LImax) at the aneurysm sac normalized by the physiological infiltration rate of the normal artery (19).

### Statistic Analysis

Clinical, morphological, hemodynamic, and LDL infiltration parameters were first examined by univariate analyses. Binary parameters were compared by the Fisher exact test. For continuous parameters, they were first examined by the Shapiro–Wilk test to determine if they were normally distributed. Student *t*-test (for normally distributed parameters) or Mann–Whitney

*U*-test (for non-normally distributed parameters) were used to identify statistically significant parameters ($P < 0.05$) between the ruptured and unruptured group. Colinearity between variables was examined by the Pearson correlation test. Receiver operating curves were plot for each significant parameter, and their corresponding area under the curve (AUC) were calculated and compared.

Only parameters that are statistically significant and independent were considered for multivariate logistic regression. A rupture prediction model was derived using a backward stepwise method.

## RESULTS

### Patient Demographics

Eighty-eight patients were included in the study, 33 of which were excluded due to missing data of lipid level or blood pressure or poor image quality. Among the 55 cases analyzed in this study, there were 62 aneurysms in total (45 unruptured and 17 ruptured). Among the 55 patients, 20 of them were male. The mean age was 58.

### Wall Shear Stress and LDL Infiltration Patterns

LDL infiltration distribution and wall shear stress distribution for typical ruptured and unruptured aneurysms are shown in **Figures 1**, **2**, respectively. In ruptured aneurysms, a high level of LDL infiltration can be observed in the sac especially in the area near bleb, while in unruptured aneurysms, infiltration flux in the aneurysm sac region was not much different from that in the artery region. Comparing the distribution of wall shear stress and LDL infiltration, we can see that high infiltration usually presented in the area characterized by excessively low wall shear stress, though the distribution patterns were different between the two.
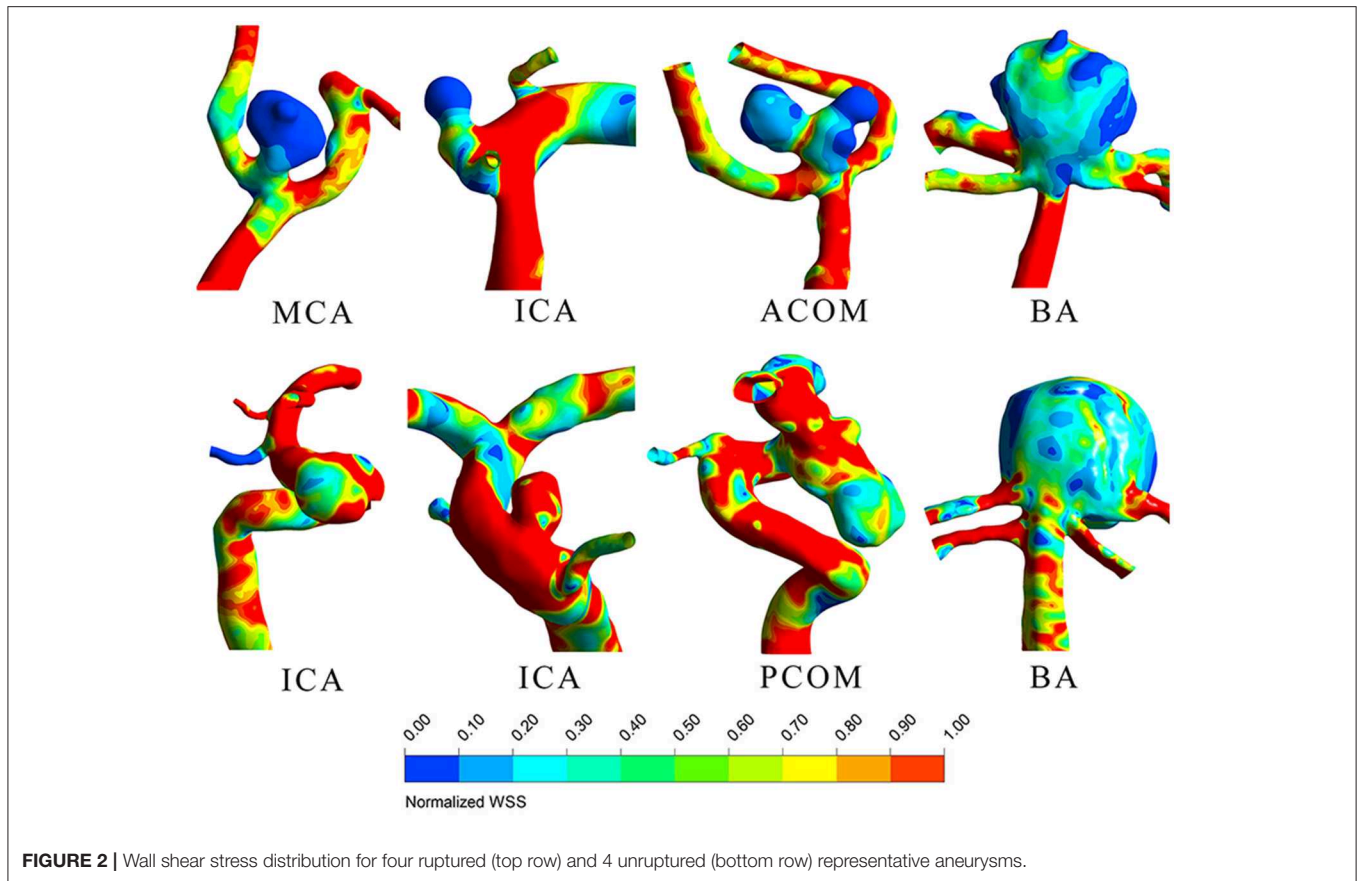
### Univariate Analyses

**Table 1** shows the means, standard deviations, and statistical results for each parameter.

For LDL infiltration parameters, both LIave and LImax were significantly higher in the ruptured group than that in the unruptured groups (LIave, $P < 0.001$, LImax, $P = 0.002$). For morphological parameters, only size ratio showed a significant difference between the ruptured and unruptured cases (2.19 vs. 1.34, $P < 0.001$). For hemodynamic parameters, significant differences were observed in wall shear stress (0.39 vs. 0.77, $P < 0.001$) and low shear area (0.26 vs. 0.09, $P < 0.001$). No significant differences were observed for LDL-c plasma level, blood pressure, sex, aneurysm size, aneurysm height, neck width, inflow artery angle, aspect ratio, and OSI. Hypertension was observed to be marginally significant ($P = 0.051$) between the two groups. Receiver operator characteristic analysis was performed for parameters with significant differences, and the result is plotted in **Figure 3**. LIave achieved the highest area under the curve (AUC) of 0.856.
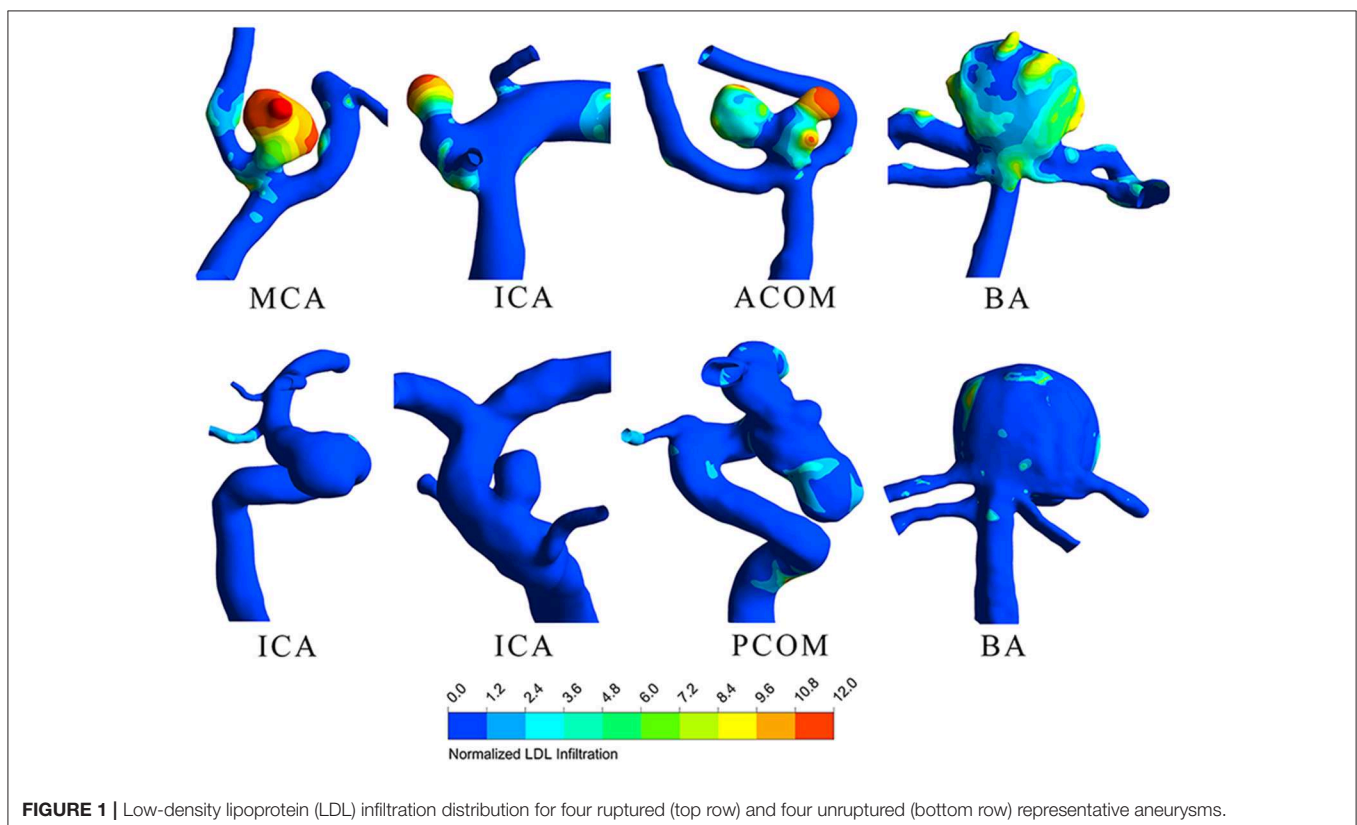


**FIGURE 1 |** Low-density lipoprotein (LDL) infiltration distribution for four ruptured (top row) and four unruptured (bottom row) representative aneurysms.

**FIGURE 2 |** Wall shear stress distribution for four ruptured (top row) and 4 unruptured (bottom row) representative aneurysms.

**TABLE 1 |** Results from univariate analysis for all parameters.

| Parameter | Ruptured ($n = 17$) | Unruptured ($n = 45$) | $P$-value |
|---|---|---|---|
| Age, year | $57.5 \pm 10.6$ | $58.3 \pm 12.1$ | 0.716 |
| Male sex | 8 (47%) | 12 (27%) | 0.125 |
| Systole, mmHg | $143 \pm 25$ | $136 \pm 24$ | 0.255 |
| Diastole, mmHg | $86 \pm 9$ | $85 \pm 11$ | 0.640 |
| Hypertension | 9 | 12 | 0.051 |
| LDL-c, mmol/L | $3.02 \pm 1.25$ | $2.63 \pm 0.80$ | 0.245 |
| Hyperlipidemia | 5 | 6 | 0.139 |
| Size, mm | $5.03 \pm 2.32$ | $5.05 \pm 4.30$ | 0.372 |
| Aneurysm height, mm | $5.14 \pm 1.44$ | $5.10 \pm 3.95$ | 0.058 |
| Aneurysm width, mm | $5.24 \pm 2.40$ | $5.84 \pm 5.28$ | 0.309 |
| Neck width, mm | $4.37 \pm 2.24$ | $4.72 \pm 3.34$ | 0.813 |
| Vessel angle, degree | $114.6 \pm 33.1$ | $104.0 \pm 29.5$ | 0.273 |
| Size ratio | $2.19 \pm 1.27$ | $1.34 \pm 0.91$ | 0.006 |
| Aspect ratio | $1.49 \pm 0.77$ | $1.12 \pm 0.56$ | 0.102 |
| WSS | $0.39 \pm 0.24$ | $0.77 \pm 0.40$ | <0.001 |
| MWSS | $1.47 \pm 0.78$ | $1.97 \pm 1.10$ | 0.116 |
| OSI | $0.033 \pm 0.018$ | $0.035 \pm 0.037$ | 0.228 |
| RRT,s | $3.44 \pm 8.81$ | $0.34 \pm 0.41$ | <0.001 |
| LSA | $0.26 \pm 0.28$ | $0.09 \pm 0.17$ | <0.001 |
| LIave | $4.71 \pm 3.81$ | $0.95 \pm 1.39$ | <0.001 |
| LImax | $11.29 \pm 6.48$ | $5.91 \pm 4.71$ | 0.002 |

**TABLE 2 |** Results from multivariate analysis for key parameters.

| Parameter | OR | 95% CI | $P$-value |
|---|---|---|---|
| LIave | 2.402 | 1.237 to 4.665 | 0.010 |
| WSS | 0.040 | 0.001 to 1.321 | 0.071 |
| LSA | 0.001 | 0.000 to 1.286 | 0.059 |

## Multivariate Regression Analyses

Colinearity between LIave, LImax, SR, WSS, LSA, and RRT were examined. Except that RRT was found to correlate with LSA (R = 0.863, $P < 0.05$), other parameters were not strongly correlated (R < 0.8). In multivariate regression analysis, LIave remained statistically significant ($P < 0.05$), as shown in **Table 2**. The odds ratio of LIave was 2.402 (1.237–4.665, 95% CI), which indicates that each unit increase in LDL infiltration will increase the risk by 2.4-fold. LSA and WSS were only marginally significant ($P = 0.059$, $P = 0.071$) in multivariate analysis. We derived a prediction model with LDL infiltration parameters and hemodynamic parameters. The receiver operator characteristic curves of the model is shown in **Figure 3**. The area under the ROC curve for the model was 0.885 (95% CI: 0.794–0.976), which indicates good discrimination between ruptured and unruptured cases.
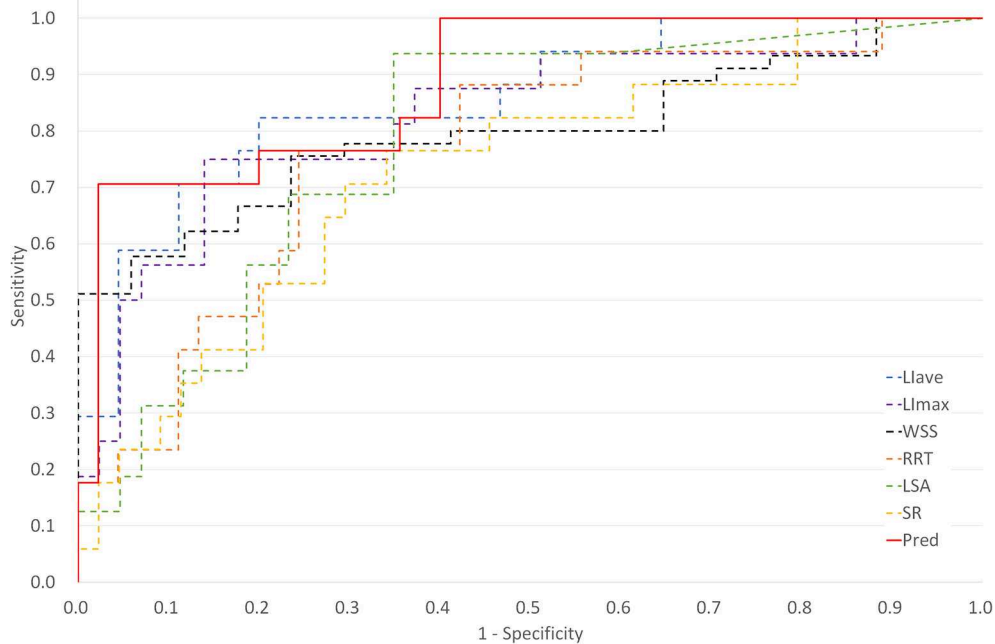
**FIGURE 3 |** Plot of receiver operating characteristic (ROC) curves for key parameters and multivariate logistic regression derived prediction model [Pred, prediction model; LIave, area averaged LDL infiltration, area under the curve (AUC) = 0.856; LImax, maximum LDL infiltration, AUC = 0.761; WSS, wall shear stress, AUC = 0.797; RRT, relative residence time, AUC = 0.761; LSA, low shear area, AUC = 0.781; SR, size ratio, AUC = 0.725].

## DISCUSSION

Our result showed that there is significantly higher LDL infiltration at the wall of ruptured aneurysm compared to unruptured ones (4.71 vs. 0.95, $P < 0.001$). Lipid accumulation in the aneurysmal wall has been shown to be associated with aneurysm rupture (9). Accumulated lipids are oxidized, and an association between oxidized LDL and the loss of mural cells and degeneration of aneurysm wall can be found. Oxidized lipids can induce chronic inflammation in atherosclerotic lesion, which is characterized by infiltration of macrophages as in ruptured aneurysm wall. Recent research has also implicated lipid accumulation as a key factor in promoting degeneration of the aneurysm wall via formation of foam cells and subsequent loss of mural cells (10, 11). In our study, higher LDL infiltration rate was observed in the ruptured aneurysm wall, implicating lipid accumulation in ruptured aneurysms, which is consistent with the above researches. Recent advance in magnetic resonance vessel wall imaging (MR-VWI) has shown association between wall enhancement and aneurysm rupture (20). Further histopathological analyses revealed that wall enhancement was associated with wall thickening with atherosclerotic change (21, 22). Our study suggested that increased lipid infiltration was associated with rupture, which was in line with these new findings from vessel wall imaging.

In our study, we also found that LDL infiltration at the sac region can be several to 10-fold higher than normal physiological value as indicated by color in **Figure 1**. This suggested that given the same patient, though parent artery and aneurysm

sac were exposed to the same plasma level of LDL, the actual LDL infiltration can vary at different locations. In some of our cases, even the patients' plasma LDL levels were within normal range, the infiltration rates at the aneurysm sac can still be much higher, which infers lipid accumulation. Our finding agrees with previous research that lipid accumulation was observed in the aneurysm wall despite normal plasma lipid level (9).

We further observed that lipid infiltration pattern was quite heterogenous at the sac region. Higher infiltration tended to appear at the tip or at blebs, as shown in **Figure 1**. As higher infiltration can lead to more extensive lipid accumulation, oxidation, and subsequent degradation of the wall at the local spot, this may explain why the rupture sites of aneurysm are usually located at the tip or bleb. The heterogenous pattern of LDL infiltration was, in part, owing to spatially varying permeability of the vessel wall, which was dependent on the local wall shear stress. We compared **Figures 1**, **2** and found out that high infiltration regions were associated with excessively low wall shear stress regions, which is consistent with literature studies that low shear stress was associated with atherosclerotic change in the aneurysm wall (23–26). Though aneurysm initiation is generally considered to be linked with high shear stress (27, 28), the role of wall shear stress in aneurysm rupture remains controversial. In some studies, the rupture sites of aneurysms were found to be associated with the low shear stress region (29, 30). Meng et al. proposed that aneurysm rupture may follow two different pathways: one is mural cell-mediated pathway and the other is inflammatory cell-mediated pathway (31). As lipid infiltration has been

recognized as the trigger for inflammation in atherosclerosis, it is possible that lipid accumulation may also promote inflammation process leading to aneurysm wall degradation and rupture.

Besides local shear stress, transmural pressure, and LDL plasma level also affect the amount of LDL infiltration. They acted as global and systemic factors on LDL accumulation, while shear stress acted as a local mediator. Lipid accumulation was the combined effect from both local factor and global factors. For example, patients having a high lipid level or high blood pressure does not necessarily indicate a high lipid accumulation in the aneurysm wall and vice versa. LDL, though widely recognized as risk factors for cardiovascular and cerebrovascular disease, was not found to be associated with cerebral aneurysm rupture in a recent clinical study (12), which seems to conflict with findings from a histopathology study (9, 10). However, it is important to note that despite LDL not recognized as a risk factor, the use of a lipid-lowering agent was found to be able to reduce the risk of rupture (12). This seemly contradiction can be explained by the intermingled effect of global factors (LDL plasma level) and local factors (WSS). As demonstrated in our result, the LDL plasma level alone cannot represent the local infiltration of LDL at the aneurysm sites, which explains why LDL plasma level did not differ significantly between ruptured and unruptured aneurysms in clinical study. Wall shear stress pattern can vary greatly between aneurysms from different patients. However, if focusing on a single patient, local factors such as shear stress will remain largely stable, the use of lipid-lowering agent can reduce plasma lipid level and alleviate lipid accumulation (by changing the global factors), therefore reducing the risk of rupture, as evident in clinical study (12). Our result can help to reconcile the different conclusions obtained from clinical study and histopathology studies.

Since the permeability of the endothelium was linked to shear stress in the model, though there was no colinearity between LIave and WSS, there is an association between these two parameters (r = 0.59, $P < 0.001$). However, since LIave was calculated with additional information from patient-specific blood pressure and plasma LDL level, it appeared to perform better than WSS alone in discriminating aneurysm rupture, as illustrated by the higher AUC achieved by LIave than in the WSS and other hemodynamic parameters.

## Limitations

All the cases were from a single center, and the number of cases is small. More cases from multiple centers should be analyzed to verify the finding. The current study was retrospective in which morphology of post-rupture aneurysms may be different from their pre-rupture shapes (32). For unruptured aneurysms, they remained unruptured during follow-up. The number of ruptured aneurysms was smaller than that of unruptured ones, which may introduce bias to our study.

As for the modeling of hemodynamics and LDL transport, there were several assumptions made. We assumed a generic

inflow waveform scaled by vessel diameters. In the model, we only considered LDL infiltration through endothelium, which is the first step of lipid accumulation. Owing to the difficulty in accurate measurement of aneurysm wall thickness, a uniform thickness was assumed (33). Nevertheless, to our best knowledge, this is the first study utilizing patient-specific modeling of LDL transport to examine the relationship between lipid transport and cerebral aneurysm rupture. An *ex vivo* histology study on resected aneurysm tissue should be conducted to validate the simulation model. Further, we can compare the simulation results with high-resolution MR-VWI images to investigate the correlation between the LDL infiltration zone and image enhancement region.

## CONCLUSIONS

We have investigated the association between lipid accumulation and cerebral aneurysm rupture using patient-specific modeling of LDL transport. Ruptured aneurysms had significantly higher LDL infiltration than unruptured ones, which suggested that lipid accumulation may promote aneurysm rupture. Lipid accumulation characteristics should be considered when assessing cerebral aneurysm rupture risk.

## DATA AVAILABILITY STATEMENT

The datasets used during the current study are available from the corresponding author on reasonable request.

## ETHICS STATEMENT

The studies involving human participants were reviewed and approved by Zhujiang Hospital. Written informed consent for participation was not required for this study in accordance with the national legislation and the institutional requirements.

## AUTHOR CONTRIBUTIONS

All authors drafted the manuscript. CO and YQ performed the simulation and analysis. XZ, JL, WL, HS, NZ, and JZ collected the data and performed data preprocessing. XH and C-ZD supervised the study.

## FUNDING

# REFERENCES

1. Li MH, Chen SW, Li YD, Chen YC, Cheng YS, Hu DJ, et al. Prevalence of unruptured cerebral aneurysms in Chinese adults aged 35 to 75 years: a cross-sectional study. *Ann Intern.* (2013) 159:514–21. doi: 10.7326/0003-4819-159-8-201310150-00004

2. Xiang J, Natarajan SK, Tremmel M, Ma D, Mocco J, Hopkins LN, et al. Hemodynamic–morphologic discriminants for intracranial aneurysm rupture. *Stroke.* (2011) 42:144–52. doi: 10.1161/STROKEAHA.110.592923

3. Varble N, Tutino VM, Yu J, Sonig A, Siddiqui AH, Davies JM, et al. Shared and distinct rupture discriminants of small and large intracranial aneurysms. *Stroke.* (2018) 49:856–64. doi: 10.1161/STROKEAHA.117.0 19929

4. Cebral JR, Mut F, Weir J, Putman C. Quantitative characterization of the hemodynamic environment in ruptured and unruptured brain aneurysms. *AJNR Am J Neuroradiol.* (2011) 32:145–51. doi: 10.3174/ajnr. A2419

5. Takao H, Murayama Y, Otsuka S, Qian Y, Mohamed A, Masuda S, et al. Hemodynamic differences between unruptured and ruptured intracranial aneurysms during observation. *Stroke.* (2012) 43:1436–9. doi: 10.1161/STROKEAHA.111.640995

6. Zhang X, Karuna T, Yao ZQ, Duan CZ, Wang XM, Jiang ST, et al. High wall shear stress beyond a certain range in the parent artery could predict the risk of anterior communicating artery aneurysm rupture at follow-up. *J Neurosurg.* (2018) 1:1–8. doi: 10.3171/2018.4.JNS173179

7. Miura Y, Ishida F, Umeda Y, Tanemura H, Suzuki H, Matsushima S, et al. Low wall shear stress is independently associated with the rupture status of middle cerebral artery aneurysms. *Stroke.* (2013) 44:519–21. doi: 10.1161/STROKEAHA.112.675306

8. Zhou G, Zhu Y, Yin Y, Su M, Li M. Association of wall shear stress with intracranial aneurysm rupture: systematic review and meta-analysis. *Sci Rep.* (2017) 7:5331. doi: 10.1038/s41598-017-05886-w

9. Frösen J, Tulamo R, Heikura T, Sammalkorpi S, Niemela M, Hernesniemi J, et al. Lipid accumulation, lipid oxidation, and low plasma levels of acquired antibodies against oxidized lipids associate with degeneration and rupture of the intracranial aneurysm wall. *Acta Neuropathol Commun.* (2013) 1:71. doi: 10.1186/2051-5960-1-71

10. Ollikainen E, Tulamo R, Lehti S, Lee-Rueckert M, Hernesniemi J, Niemela M, et al. Smooth muscle cell foam cell formation, apolipoproteins, and ABCA1 in intracranial aneurysms: implications for lipid accumulation as a promoter of aneurysm wall rupture. *J Neuropath Exp Neur.* (2016) 75:689–99. doi: 10.1093/jnen/nlw041

11. Ollikainen E, Tulamo R, Lehti S, Hernesniemi J, Niemela M, Kovanen PT, et al. Myeloperoxidase associates with degenerative remodeling and rupture of the saccular intracranial aneurysm wall. *J Neuropath Exp Neur.* (2018) 77:461–8. doi: 10.1093/jnen/nly028

12. Can A, Castro VM, Dligach D, Finan S, Yu S, Gainer V, et al. Lipid-lowering agents and high HDL (high-density lipoprotein) are inversely associated with intracranial aneurysm rupture. *Stroke.* (2018) 49:1148–54. doi: 10.1161/STROKEAHA.117.019972

13. Sakellarios A, Bourantas CV, Papadopoulou SL, Tsirka Z, de Vries T, Kitslaar PH, et al. Prediction of atherosclerotic disease progression using LDL transport modelling: a serial computed tomographic coronary angiographic study. *Eur Heart J Cardiovasc Imaging.* (2016) 18:11–8. doi: 10.1093/ehjci/jew035

14. Sakellarios AI, Räber L, Bourantas CV, Exarchos TP, Athanasiou LS, Pelosi G, et al. Prediction of atherosclerotic plaque development in an *in vivo* coronary arterial segment based on a multilevel modeling approach. *IEEE Trans Bio Med Eng.* (2016) 64:1721–30. doi: 10.1109/TBME.2016.26 19489

15. Dhar S, Tremmel M, Mocco J, Yamamoto J, Siddiqui AH, Hopkins LN, et al. Morphology parameters for intracranial aneurysm rupture risk assessment. *Neurosurgery.* (2008) 63:185–97. doi: 10.1227/01.NEU.0000316847.64140.81

16. Olgac U, Poulikakos D, Saur SC, Alkadhi H, Kurtcuoglu V. Patient-specific three-dimensional simulation of LDL accumulation in a human left coronary artery in its healthy and atherosclerotic states. *Am J Physiol Heart Circ.* (2009) 296:H1969–82. doi: 10.1152/ajpheart.01182.2008

17. Olgac U, Knight J, Poulikakos D, Saur SC, Alkadhi H, Desbiolles LM, et al. Computed high concentrations of low-density lipoprotein correlate with plaque locations in human coronary arteries. *J Biomech.* (2011) 44:2466–71. doi: 10.1016/j.jbiomech.2011. 06.022

18. Jesionek K, Slapik A, Kostur M. Low-density lipoprotein transport through an arterial wall under hypertension–a model with time and pressure dependent fraction of leaky junction consistent with experiments. *J Theor Biol.* (2016) 411:81–91. doi: 10.1016/j.jtbi.2016. 09.020

19. Deng X, Marois Y, How T, Merhi Y, King M, Guidoin R. Luminal surface concentration of lipoprotein (LDL) and its effect on the wall uptake of cholesterol by canine carotid arteries. *J Vasc Surg.* (1995) 21:135–45. doi: 10.1016/S0741-5214(95)70252-0

20. Edjlali M, Gentric JC, Régent-Rodriguez C, Trystram D, Hassen WB, Lion S, et al. Does aneurysmal wall enhancement on vessel wall MRI help to distinguish stable from unstable intracranial aneurysms? *Stroke.* (2014) 45:3704–6. doi: 10.1161/STROKEAHA.114.0 06626

21. Shimonaga K, Matsushige T, Ishii D, Sakamoto S, Hosogai M, Kawasumi T, et al. Clinicopathological insights from vessel wall imaging of unruptured intracranial aneurysms. *Stroke.* (2018) 49:2516–9. doi: 10.1161/STROKEAHA.118.021819

22. Hudson JS, Zanaty M, Nakagawa D, Kung DK, Jabbour P, Samaniego EA, et al. Magnetic resonance vessel wall imaging in human intracranial aneurysms: histological analysis. *Stroke.* (2019) 50:e1. doi: 10.1161/STROKEAHA.118.023701

23. Sugiyama S-i, Niiuma K, Nakayama T, Shimizu H, Endo H, Inoue T, et al. Relative residence time prolongation in intracranial aneurysms: a possible association with atherosclerosis. *Neurosurgery.* (2013) 73:767–76. doi: 10.1227/NEU.0000000000000096

24. Jiang P, Liu Q, Wu J, Chen X, Li M, Yang F, et al. Hemodynamic findings associated with intraoperative appearances of intracranial aneurysms. *Neurosurg Rev.* (2018) 43:1–7. doi: 10.1007/s10143-018-1027-0

25. Cebral JR, Detmer F, Chung BJ, Choque-Velasquez J, Rezai B, Lehto H, et al. Local hemodynamic conditions associated with focal changes in the intracranial aneurysm wall. *AJNR Am J Neuroradiol.* (2019) 40:510–6. doi: 10.3174/ajnr.A5970

26. Tateshima S, Tanishita K, Omura H, Sayre J, Villablanca JP, Martin N, et al. Intra-aneurysmal hemodynamics in a large middle cerebral artery aneurysm with wall atherosclerosis. *Surg Neurol.* (2008) 70:454–62. doi: 10.1016/j.surneu.2008.03.035

27. Kulcsár Z, Ugron A, Marosfoi M, Berentei Z, Paál G, Szikora I, et al. Hemodynamics of cerebral aneurysm initiation: the role of wall shear stress and spatial wall shear stress gradient. *AJNR Am J Neuroradiol.* (2011) 32:587–94. doi: 10.3174/ajnr.A2339

28. Zhang X, Yao Z-Q, Karuna T, He XY, Wang XM, Li XF, et al. The role of wall shear stress in the parent artery as an independent variable in the formation status of anterior communicating artery aneurysms. *Eur Radiol.* (2019) 29:689–98. doi: 10.1007/s00330-018-5624-7

29. Kadasi LM, Dent WC, Malek AM. Colocalization of thin-walled dome regions with low hemodynamic wall shear stress in unruptured cerebral aneurysms. *J Neurosurg.* (2013) 119:172–9. doi: 10.3171/2013.2.JNS 12968

30. Suzuki T, Stapleton CJ, Koch MJ, Tanaka K, Fujimura S, Suzuki T, et al. Decreased wall shear stress at high-pressure areas predicts the rupture point in ruptured intracranial aneurysms. *J Neurosurg.* (2019) 1:1–7. doi: 10.3171/2018.12.JNS 182897

31. Meng H, Tutino V, Xiang J, Siddiqui A. High WSS or low WSS? Complex interactions of hemodynamics with intracranial aneurysm initiation, growth, and rupture: toward a unifying hypothesis. *AJNR Am J Neuroradiol.* (2014) 35:1254–62. doi: 10.3174/ajnr.A3558

32. Skodvin TØ, Johnsen L-H, Gjertsen Ø, Isaksen JG, Sorteberg A. Cerebral aneurysm morphology before and after rupture: nationwide case series of

29 aneurysms. *Stroke.* (2017) 48:880–6. doi: 10.1161/STROKEAHA.116.0
15288

33. Torii R, Oshima M, Kobayashi T, Takagi K, Tezduyar TE. Numerical
investigation of the effect of hypertensive blood pressure on cerebral
aneurysm—dependence of the effect on the aneurysm shape. *Int J Numer
Methods Fluids.* (2007) 54:995–1009. doi: 10.1002/fld.1497

**Disclaimer:** The data in this study has been anonymized. Written informed
consent was waived by the Institutional Review Board. The authors report no
conflict of interest concerning the materials or methods used in this study or the
findings specified in this paper.